

# Tribological, Mechanical, and Thermal Behavior of Titanium Dioxide and Graphene Nanoplatelet Embedded Epoxy Based Hybrid Nanocomposite

Shubham<sup>a,\*</sup>, Palak Bharti<sup>a</sup>, Rajesh Kumar Prusty<sup>a</sup>, and Bankim Chandra Ray<sup>a</sup>

<sup>a</sup>FRP Composite Laboratory, Department of Metallurgical and Materials Engineering,  
National Institute of Technology, Rourkela, 769008 India

\*e-mail: nitr.shubham@gmail.com

Received May 18, 2022; revised July 15, 2022; accepted August 10, 2022

**Abstract**—This article deals with the influence of titanium dioxide (TiO<sub>2</sub>) and graphene nanoplatelet (GnP) on epoxy's tribological, compressive, surface hardness and thermal response. Initially, the TiO<sub>2</sub> and GnP particle morphology was analyzed. A ball-on-disc testing apparatus was used to evaluate the wear and frictional behavior of the nanocomposites. The worn-out surface micrographs of tested nanocomposite samples were analyzed using a scanning electron microscope (SEM). The compressive response of the nanocomposite samples was analyzed at in-situ temperatures of 30, 75 and 120°C. The hardness of the nanocomposite sample's surface was also examined, along with the influence of nanofiller addition on samples' glass transition temperature ( $T_g$ ). The elemental-colored mapping was used to verify the proper dispersion of the nanofiller in the epoxy. It was observed that the inclusion of 2 phr (per hundred resin) by weight of TiO<sub>2</sub> along with 2 phr GnP showed a decrement of 65.17% in wear volume and an increase of 17.37% peak compressive stress value at 30°C compared to neat epoxy. An increment in the  $T_g$  was also observed with the inclusion of nanofillers in epoxy. Significant outcomes of the study conducted on the nanocomposite samples are discussed in this article.

DOI: 10.1134/S0965545X22700328

## INTRODUCTION

Epoxy resins have been extensively studied during the last few decades due to their widespread application [1, 2]. They are widely recognized for their brittleness and low resistance to fracture initiation and propagation. As a result, researchers have concentrated on strategies to increase epoxy's fracture resistance (toughness and brittleness) [3, 4]. The inclusion of nanofillers in polymer composites has shown immense credibility in enhancing its mechanical (including toughness), thermal, rheological, optical characteristics and electrical behavior [5]. Incorporating nanoparticles such as silica (SiO<sub>2</sub>), titanium dioxide (TiO<sub>2</sub>), alumina (Al<sub>2</sub>O<sub>3</sub>), carbon black, carbon nanotubes (CNTs), graphene and nanoclay into the polymer matrix, is one of the most explored approaches to advance the mechanical properties of the polymer composites even with relatively little concentration. These nanocomposites are a substitute for metal-based materials. They have many possibilities as multifunctional materials for an extensive range of applications such as civil engineering, automotive, aerospace, optoelectronic devices, and semiconductor devices [6, 7].

One commonly used nanofiller by researchers in polymer matrix composites is TiO<sub>2</sub> [8–10]. It facilitates the creation of high-performance and malleable polymer networks (for instance, obtaining filaments for 3D printing and improving viscosity). Due to its non-toxicity, chemical inertness properties, high refractive index, low cost, and other advantageous surface properties, TiO<sub>2</sub> is used in various applications, including antibacterial and antiseptic configurations and degrading organic contaminants and germs, and as a UV-resistant material. TiO<sub>2</sub> nanoparticles incorporated into multiple forms of the polymeric matrix can have synergistic effects. The effect of TiO<sub>2</sub> nanoparticles on numerous properties of polymeric composites has been studied by various researchers earlier, primarily to determine whether the application is feasible.

Similarly, graphenes have been effectively employed in composite materials, significantly increasing their thermal conductivity. Its remarkable thermal characteristics are ascribed to features such as high aspect ratio, stiffness, two-dimensional geometry, and low thermal interface resistance [11, 12]. Graphene nanoplatelet (GnP) as an epoxy matrix reinforcement shows exceptional mechanical and

electrical qualities and possesses a large specific surface area. In our previous study [13], it was observed that the addition of 0.5 phr GnP to the Kevlar/epoxy composite enhances the interlaminar shear strength (ILSS) of the laminated composite by 12.5% at room temperature. Cilento et al. [14] examined how the amount of GnPin a GnP/epoxy nanocomposite affected the reinforcing efficiency. Wang et al. [15] added 0.5 vol percent GnP into poly(vinyl alcohol) (PVA), which led to a 91.1% improvement in tensile strength and a 66.7% rise in Young's modulus compared to neat PVA [16].

Enhancement of properties by adding the nanomaterials in polymer resin is generally attributed to the development of much better molecular interactions between them and the polymer matrix. The dispersion of nanofillers in a homogeneous manner into the polymer matrix for achieving high performance and superior characteristics is vital [17]. In recent times, the use of binary nanofiller is growing due to their remarkable synergetic effect. In other words, binary nanofiller addition in polymer results in more pronounced properties of nanocomposites because of the various interactions of different nanofillers with the polymers. The increased surface-to-volume ratio of nanofillers provides more surface for contact and is the key to these interactions [18]. Sumfleth et al. [19] explained a new method for improving carbon nanotube dispersion by adding a second type of nanoparticle (titania), which forms the third phase. As per their study, the improved dispersion paired with better physical characteristics owing to synergistic effects is one of the key advantages of such multiphase systems. Synergistic effects are frequently linked to a change in one or both types of particles' state of dispersion. Interactions between fillers and/or matrix might vary depending on the kind of filler. Microscale particles having a hybrid structure are used in traditional multiphase systems. Nuruddin et al. [20] studied an epoxy polymer composite made using binary filler materials, graphene nanoplatelets and montmorillonite nanoclay (MMT). To examine the synergistic influence of nanofillers on composite characteristics, different loading percentages of individual and binary nanofillers were integrated into an epoxy matrix system by them. The viscoelastic and flexural characteristics of plain epoxy and nanofillers reinforced nanocomposites were investigated by them using dynamic mechanical analysis (DMA) and a three-point bend test. They observed no significant change in glass transition temperature, including 3 wt % MMT and 0.1 wt % graphene nanoplatelets resulted in improved flexure modulus, strength and storage modulus.

Mechanical characterizations of the polymer composite samples are essential steps that need to be undertaken before the final application of the material in commercial use. Wear is often assumed to be among the most common reasons for failure in many engineering applications. Tribological studies of any mate-

rial generally concentrate on its surface damage in terms of material-removal mechanisms, such as transfer film, plastic deformation, tribochemistry, and brittle fracture. Wear occurs even to the hardest materials, including diamonds [21]. Standard test procedures such as ball-on-disc and pin-on-disc are widely utilized to replicate rubbing action in which plastic yielding occurs at the tip of individual asperities. In machining processes, lowering the coefficient of friction (CoF) has numerous benefits. The main goal of conducting wear tests is to provide tribologists with the information needed to choose the design's optimal material.

Another critical aspect of a material is the surface hardness and the material's response to thermal conditions. In the microhardness test, an indenter (Berkovich or Vickers) is impressed using a known applied load into the test specimen surface. Loading to a maximum load, maintaining at the maximum load for a brief period and unloading back to zero load are the three components of a typical load-indentation depth curve. To avoid time-dependent effects, a 10-second holding interval was used. The impression dimensions on the sample along the diagonals are measured to know the hardness  $H_v$  of the material in the Vickers microhardness test setup. For the thermal characterization of the polymer composite sample,  $T_g$  assessment is considered critical. The effect of the nanofillers' size and dispersion conditions on the glass-transition temperature have been studied by various researchers [22–24].  $T_g$  is one parameter that specifies a material tolerance to a temperature higher than room temperature. The glass transition behaviors of any material can be investigated using differential scanning calorimetry (DSC).

In this study, epoxy resin is modified using binary nanofillers that involve  $\text{TiO}_2$  and GnP. The amount of  $\text{TiO}_2$  was kept at 2 phr in all the cases, whereas GnP content was varied as 0, 1 and 2 phr. The neat epoxy sample was taken as a reference. The  $\text{TiO}_2$  and GnP particle's morphology was analyzed using a high-resolution transmission electron microscope (HRTEM) and field emission-scanning electron microscope (FE-SEM). The tribological behavior of the nanocomposite samples was analyzed on the ball-on-disc apparatus. The load was kept constant at 50 N, and the test was carried out for 1260 s. SEM micrography was used to analyze the worn-out surface of the tested samples. The nanocomposite's peak stress (compressive) values were analyzed at in-situ temperatures of 30, 75, and 120°C using a universal testing machine (UTM). The surface hardness was also measured using the Vickers microhardness apparatus. The thermal behavior of the samples was analyzed using DSC. The dispersion of the nanofillers in the nanocomposite samples was checked using the EDX elemental-colored mapping. Finally, the relevant outcomes were discussed thoroughly in this article.

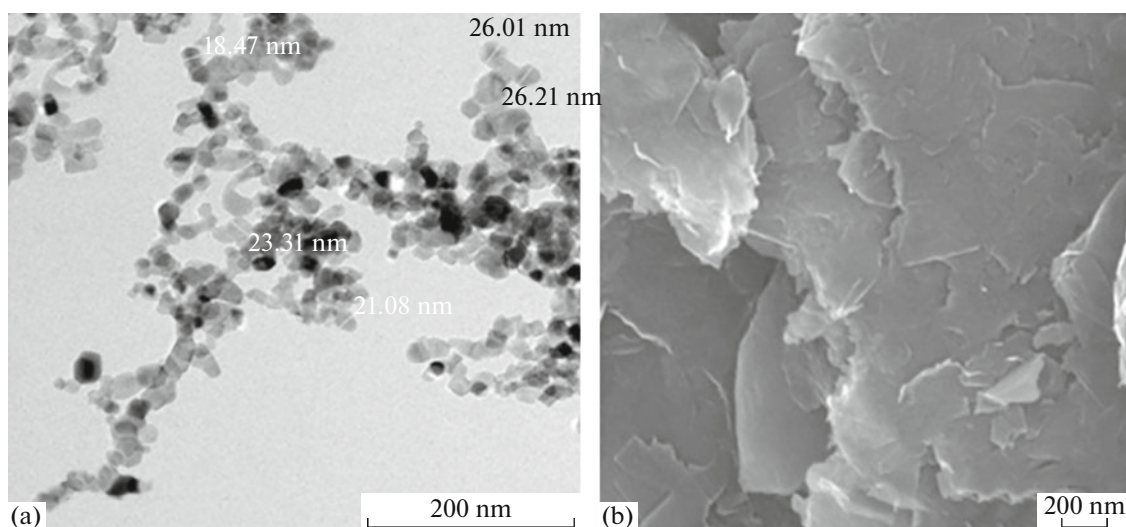


**Fig. 1.** Nanoscale images of the (a)  $\text{TiO}_2$  particles and (b) GnP used in this study.

## EXPERIMENTAL

### *Materials Specification and Nanofiller Morphology*

In this experimentation, samples were fabricated using an intermediate viscosity, liquid epoxy resin based on Bisphenol-A resin, and triethylenetetramine as a hardening agent, both commercially known as Lapox L-12 and K6, respectively. Atul Industries, India, provided these chemicals. Epoxy had a density of  $1.1\text{--}1.2\text{ g/cm}^3$  and a viscosity of  $9000\text{--}12000\text{ mPa s}$  at  $25^\circ$ . The fillers used in this study were GnP and Titanium (IV) oxide ( $\text{TiO}_2$ ) obtained from Sigma-Aldrich company. As per the manufacturer, the GnP provided is a low-dimensional carbon nanoplatelet that is a few layers thick. It is slightly oxidized (the oxygen content is around 1%), yielding a superior dispersion behavior in different solvent/matrices. Figures 1a and 1b show the high-resolution transmission electron microscope (HRTEM) image of the  $\text{TiO}_2$  fillers and the field emission-scanning electron microscope (FESEM) image of the GnP particles used. The morphology of the  $\text{TiO}_2$  particles was observed to be near about spherical with an average diameter of around 22 nm. The GnP showed a flaky structure of the individual particle.

### *Nanocomposite Fabrication*

In this work, four different types of epoxy-based nanocomposites were fabricated by integrating magnetic stirring and ultrasonic dispersion methods. According to the available literature [25], adding  $\text{TiO}_2$  up to 2 phr improves the functional capabilities of the base material; however, any further increase in  $\text{TiO}_2$  may result in a decrease in their intrinsic properties. With these concerns in mind, the weight percent of

$\text{TiO}_2$  in this study was likewise kept constant (2 phr). Samples prepared were neat epoxy,  $\text{TiO}_2$  (2 phr) modified epoxy and  $\text{TiO}_2$  (2 phr) along with GnP (1 phr and 2 phr) modified epoxy. Sample codes for different configurations have been given in Table 1.

For the fabrication of  $\text{TiO}_2$  modified epoxy samples, the required amount of epoxy was stirred using a magnetic bead at 400 rpm for 30 min at a temperature of  $120^\circ\text{C}$ . After that,  $\text{TiO}_2$  (dried) in powder form was added to the flask containing epoxy, and again this mixture was stirred using a magnetic bead at 1000 rpm for 1 hr at  $120^\circ\text{C}$ . Then the  $\text{TiO}_2$ /epoxy mixture was ultra-sonicated for 1 hour at room temperature. There is a strong possibility that air bubbles will get trapped inside the suspension while performing these processes. Hence the suspension was vacuum degassed for 18 hours to avoid such occurrence. After that,  $\text{TiO}_2$ /epoxy suspension and hardener (10 phr) were poured into the mold and well mixed by stirring. The amount of hardener added in this study was as per the resin manufacturer. It was then allowed to solidify at room temperature and left for 24 h. Final samples were prepared from the mold and post-cured at  $140^\circ\text{C}$  for

**Table 1.** Sample codes for nanocomposites with different amounts of GnP

Sample Configuration	Sample Code
Neat epoxy	NE
Epoxy + 2 phr $\text{TiO}_2$ + 0 phr GnP	E-2T
Epoxy + 2 phr $\text{TiO}_2$ + 1 phr GnP	E-2T-1G
Epoxy + 2 phr $\text{TiO}_2$ + 2 phr GnP	E-2T-2G

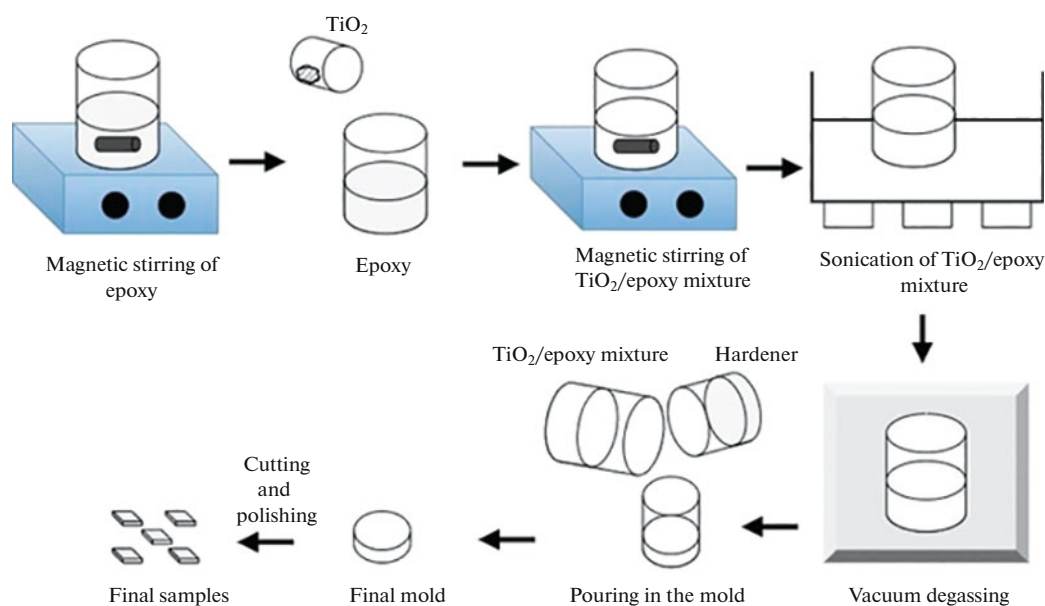


Fig. 2. Schematic diagram of fabrication of single nanofiller composite.

6 h in a hot air oven. The samples were allowed to cool down in the oven itself before being tested. Figure 2 depicts the schematic of the procedure followed to prepare the TiO<sub>2</sub> embedded epoxy samples.

The preparation of homogeneous epoxy-binary nanofiller suspension involves several complex steps which are shown schematically in Fig. 3. At first, a magnetic bead was used to stir the mixture containing GnP in the appropriate phr in acetone at 1000 rpm for 30 minutes at room temperature. The GnP/acetone suspension was then ultrasonicated at room temperature for 30 minutes. At the same time, the required amount of epoxy was stirred at 400 rpm for 30 min at 120°C using a magnetic bead, and the weight of the whole flask was measured. After that, the GnP/acetone mixture was added to the flask containing epoxy. The GnP/acetone/epoxy mixture was then stirred again with a magnetic bead at 1000 rpm at 120°C until the acetone had fully evaporated. Weighing the mixture at frequent intervals ensures that the acetone has completely evaporated. After the acetone had evaporated entirely, TiO<sub>2</sub> (dry) powder was added to the flask containing the GnP/epoxy combination. Again, this mixture was stirred using a magnetic bead at 1000 rpm for 1 h at 120°C. After this, TiO<sub>2</sub>/GnP/epoxy suspension was subjected to ultrasonication for 1 hr at room temperature to enhance the dissolution and prevent the agglomeration of nanofillers into the epoxy. After that, the suspension was subjected to vacuum degassing for 18 hours. The process for the sample fabrication was then followed, as mentioned for TiO<sub>2</sub> embedded epoxy samples.

#### Characterizations of Material

**Tribological Testing.** A ball-on-disc frictional test was performed to get the wear and frictional behavior of the nanocomposites. A steel ball having a diameter of 2 mm was used for the same with a load of 50 N. Figure 4 shows the test setup used for the study. The track diameter was 8 mm, and the wear time was 1260 s. Wear rate concerning time and wear rate concerning distance was obtained by dividing wear volume by time and distance of wear. The specific wear rate  $W_s$ , which defines the wear performance under the given parameters for a tribosystem, was obtained using Eq. (1).

$$W_s = \frac{\Delta V}{F_N d} \text{ [mm}^3\text{/(Nm)]}, \quad (1)$$

where  $F_N$  is the normal force exerted on the steel ball during sliding, and  $d$  is the total sliding distance. At least five repetitive tests were done for each test condition.

The coefficient of friction was obtained by dividing frictional force with normal force.

**Mechanical and thermal testing.** Figure 5 shows the experimental setup used to analyze different nanocomposite samples' mechanical and thermal characteristics. For compression loading, cylindrical specimens were prepared to have a diameter of 8 mm and a length of 6 mm. To avoid buckling, the compression specimen size was chosen at a short length. These tests were carried out on an Instron 5967 universal testing machine with a 1 mm/min cross-head speed. Peak stress (engineering) values under compressive loading conditions were obtained. Specimens were tested at

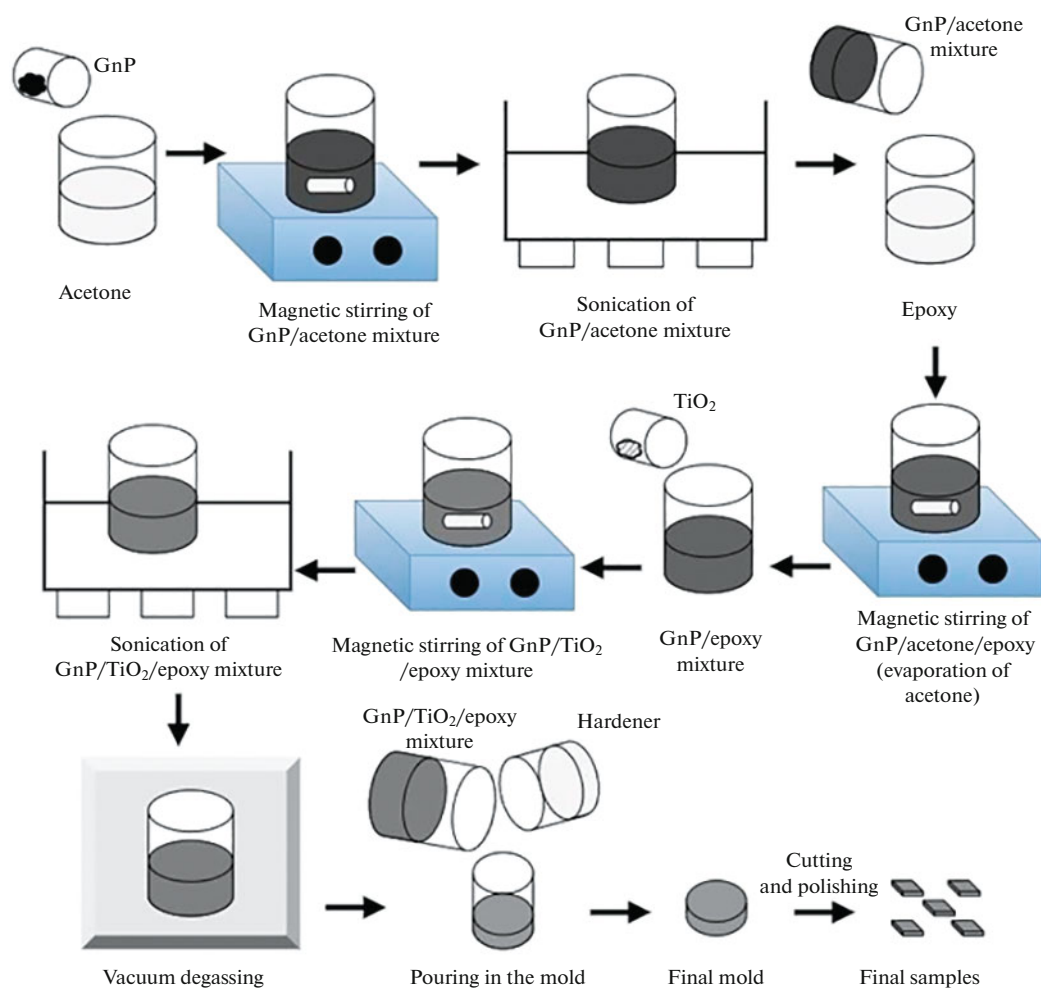


Fig. 3. Schematic diagram of fabrication of binary nanofiller composite.

three different in-situ temperatures (30, 75, and 120°C), and average peak stress values along with respective standard deviations were plotted.

The micro Vickers hardness testing machine was used to determine the surface hardness of the nanocomposite samples. The diamond indenter is pressed into the sample's surface to conduct the experiment. The indenter is pyramid-shaped with a square base and a 136-degree angle between opposite faces. In this study, a 100 gf (gram force) load was applied for 10 s.

In order to determine the thermal effect of TiO<sub>2</sub>+GnP addition in epoxy, differential scanning calorimetry (DSC) analysis was carried out on NE, E-2T, E-2T-1G, and E-2T-2G nanocomposites. The temperature range of the analysis was 40 to 200°C at a heating rate of 10 grad/min using Mettler Toledo (DSC 822) to determine the glass transition temperature  $T_g$  of the composites. About five samples of each configuration were tested for  $T_g$  analysis.

**Optical and electron microscopy.** A stereo microscope was used to capture the track width of the wear-

tested samples. The worn-out sample surface and the fractured samples during the compression test were analyzed using SEM, and the dispersion of the nanofillers in the matrix was observed using the EDX analysis. When SEM is used to take a micrograph to detect the elemental composition of a sample, EDX spectroscopy is used. EDX can classify elements with an atomic number in case it is greater than boron, and these elements can be recognized in concentrations of at least 0.1%. Spot detection analysis of regions up to 10 cm in diameter, contaminant identification, material evaluation and identification, quality control screening, and other applications are possible with EDX.

## RESULTS AND DISCUSSION

### *Ball-on-disc Wear Analysis*

The tribological properties of the TiO<sub>2</sub> and GnP reinforced epoxy-based nanocomposites under normal loading conditions were investigated. Although the applied load to the samples is constant, the maxi-

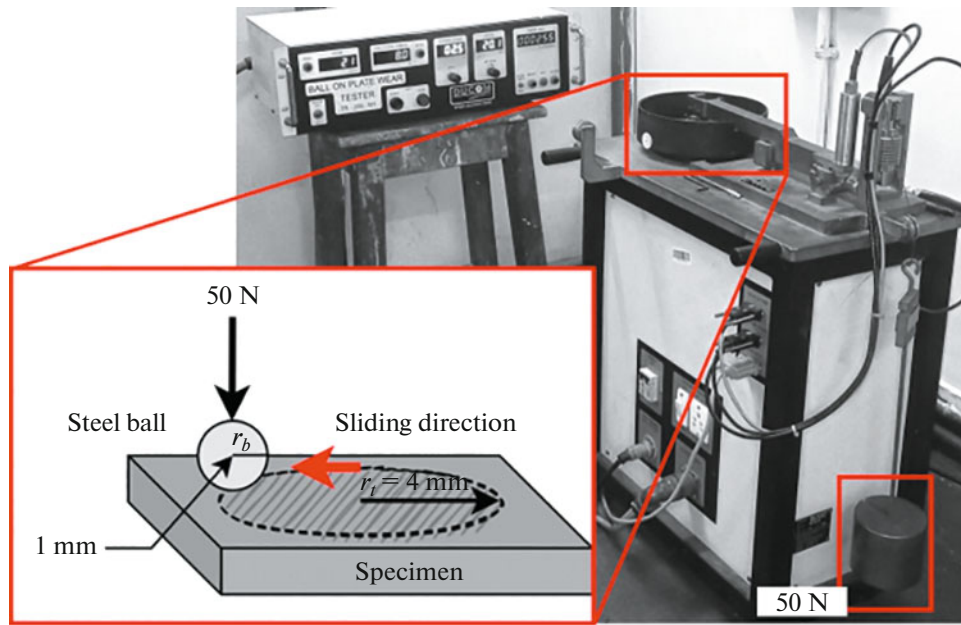


Fig. 4. Experimental setup along with schematic diagram of the ball-on-disc sliding test.

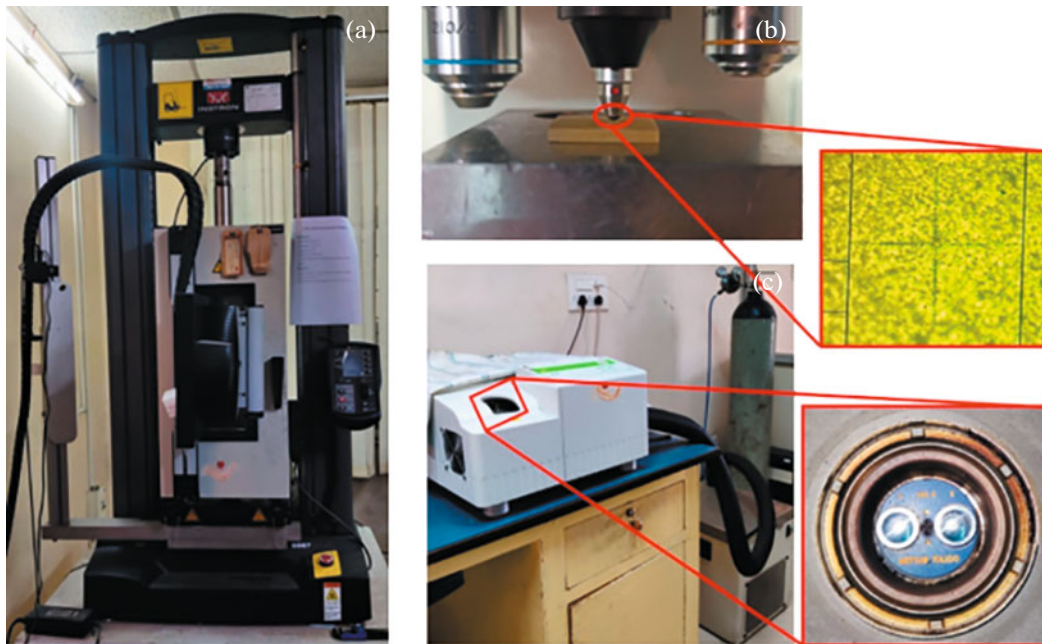
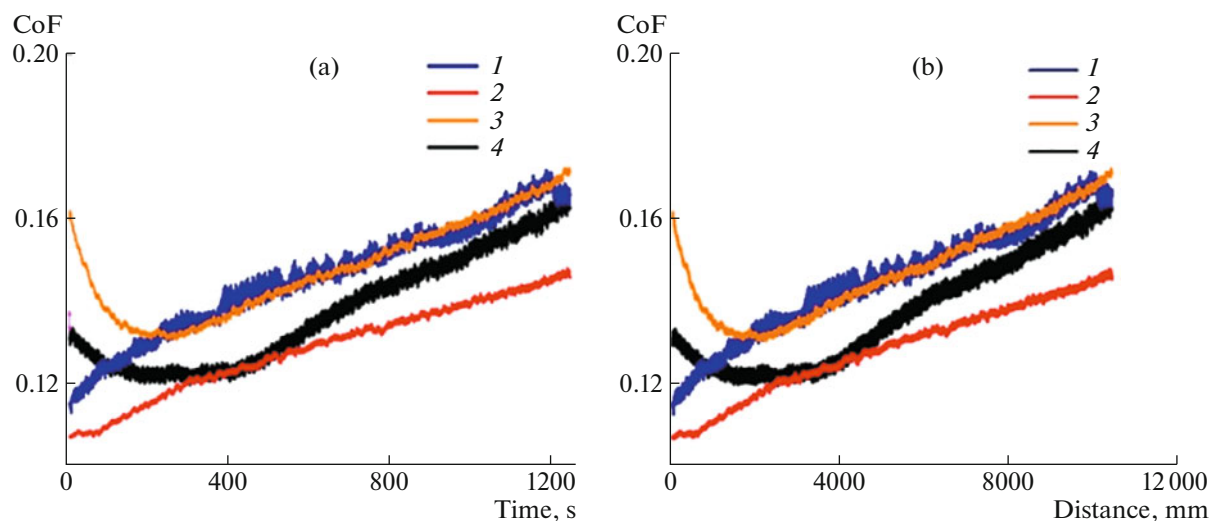


Fig. 5. (a) compression testing using UTM, (b) experimental setup of microhardness test, (c) thermal analysis using DSC.

mum shear stress and contact surface pressure on the contact surfaces change with the modulus of elasticity and Poisson’s ratios of the samples. The samples’ wear and friction characteristics were examined at 50 N normal force, 8.377 mm/s sliding speed, for 1260 s sliding duration. Figures 6a, 6b show typical CoF vs. sliding time and CoF vs. sliding distance graphs for the samples. The neat epoxy sample displays a rise in CoF

value at the start of sliding wear (running-in), likely due to the steadily expanded contact area between friction pairs. In comparison, the CoF values decrease on adding TiO<sub>2</sub> nanoparticles into the epoxy resin. Nanocomposite samples containing the GnP particles initially showed a decrease in CoF value followed by an increase. The initial decline in E-2T-1G and E-2T-2G samples can be attributed to an increase



**Fig. 6.** The friction coefficient as a function of (a) sliding time and (b) sliding distance: (1) NE, (2) E-2T, (3) E-2T-1G, (4) E-2T-2G.

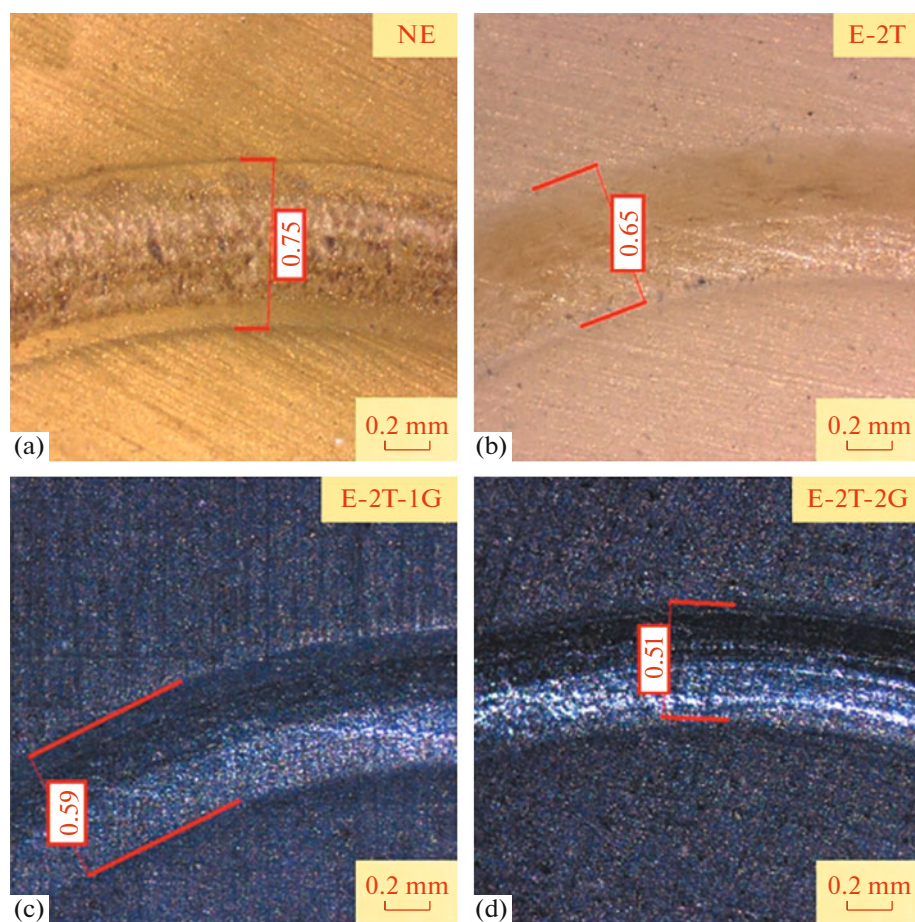


**Fig. 7.** Wear track width observed using an optical microscope of (a) NE, (b) E-2T, (c) E-2T-1G, and (d) E-2T-2G.

in surface hardness due to the addition of GnP. There is a very slight difference in the nanocomposite samples' CoF values, and the value remained in the range of 0.1-0.17.

Figure 7 shows the wear track images of tested samples having different configurations using an optical microscope. The neat epoxy sample was observed to have maximum track width compared to the nano-

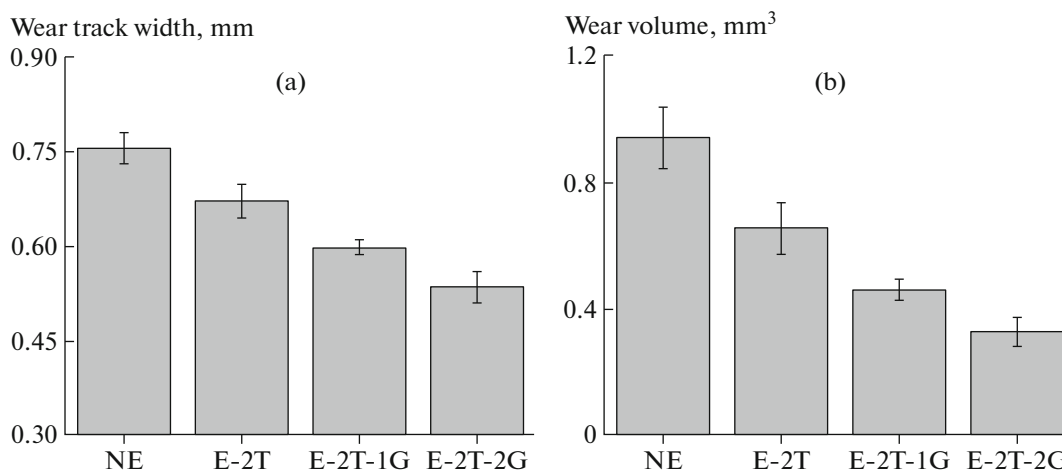


Fig. 8. Plot of (a) wear track width and (b) wear volume for different nanocomposite samples.

composite samples. Figure 8a shows the mean track width values of NE, E-2T, E-2T-1G, and E-2T-2G. On addition of 2 phr  $\text{TiO}_2$ , there is a decrement of 13.3% in the track width as compared to neat epoxy. Further, the addition of GnP (1 and 2 phr) along with 2 phr  $\text{TiO}_2$  decreased the track widths by 21.3 and 42.7%, respectively. The wear volume for different nanocomposite samples is shown in Fig. 8b. Significant decrement was observed for the same. The E-2T sample showed a 30.3% decrease in wear volume. The decline was further enhanced by the addition of GnP (1 and 2 phr) along with 2 phr  $\text{TiO}_2$ , which accounted for 50.9 and 65.1% when compared with neat epoxy.

The cumulative wear rate obtained experimentally was determined for the nanocomposites by dividing the corresponding wear volume by time and distance of wear, as shown in Figs. 9a, 9b. The reduction % in the cumulative wear rates for the nanocomposites samples was similar to the reduction % discussed for the wear volume. Literature [25–28] suggests the addition of  $\text{TiO}_2$  improves the mechanical characteristics of the nanocomposite sample. Hence this study result indicates that the good mechanical properties of nanocomposites containing nanofillers are in line with their improved wear resistance. Figure 9c shows the cumulative specific wear rate for the nanocomposite samples. The amount of GnP was not increased further as the wear resistance may be lowered if the quantity of GnP surpasses the limit set in this investigation. Here are some possible explanations. The GnPs adsorbed on an extensive specific surface of the epoxy matrix. As a result, the epoxy matrix can only contain a limited quantity of GnP. GnP aggregates will develop at high concentrations. This indicates that when the content of GnP increases, the dispersion of GnP will worsen. As a result, weak surfaces will emerge, and composites subjected to frictional stress

will be more easily damaged, resulting in a greater specific wear rate (namely, a further reduction in tribological performance). Further explanation is provided in section 3.7 using the EDX analysis.

#### Micrograph Analysis of Worn-out Surface

The shear stress is most significant at the surface due to the high friction between sliding contacts. Repetitive sliding of the steel ball creates wear debris (via adhesive wear) in this test due to the enormous shear forces induced at the surface. The production of miniature waves (Fig. 10a), i.e., neat epoxy, can be described in the following way during the wear test, the steel ball repeatedly slides under high normal loads, causing cyclic stress concentration in front of the steel ball, resulting in surface fatigue. This surface fatigue causes minute fractures in the epoxy's surface and subsurface, propagating parallel and perpendicularly to the sliding direction. The creation of microcracks network eventually results in the formation of microscopic wave-type structures on the wear track [29].

On the other hand, the epoxy samples with nanofillers have relatively smooth worn surfaces (Figs. 10b, 10c). Furthermore, appropriate nanoparticle dispersion inside the epoxy resin may have improved the nanocomposite's strength by transmitting stresses from the epoxy to the nanoparticle network. The addition of  $\text{TiO}_2$  along with GnP into epoxy shows the highest wear resistance (Fig. 10c).

#### In situ Elevated Temperature Compression Analysis

Figure 11 shows a comparison of compressive peak engineering stress values of NE, E-2T, E-2T-1G and E-2T-1G samples at various temperatures. On adding  $\text{TiO}_2$  along with GnP (0, 1 and 2 phr) to the epoxy resin at ambient temperature, It was found that the



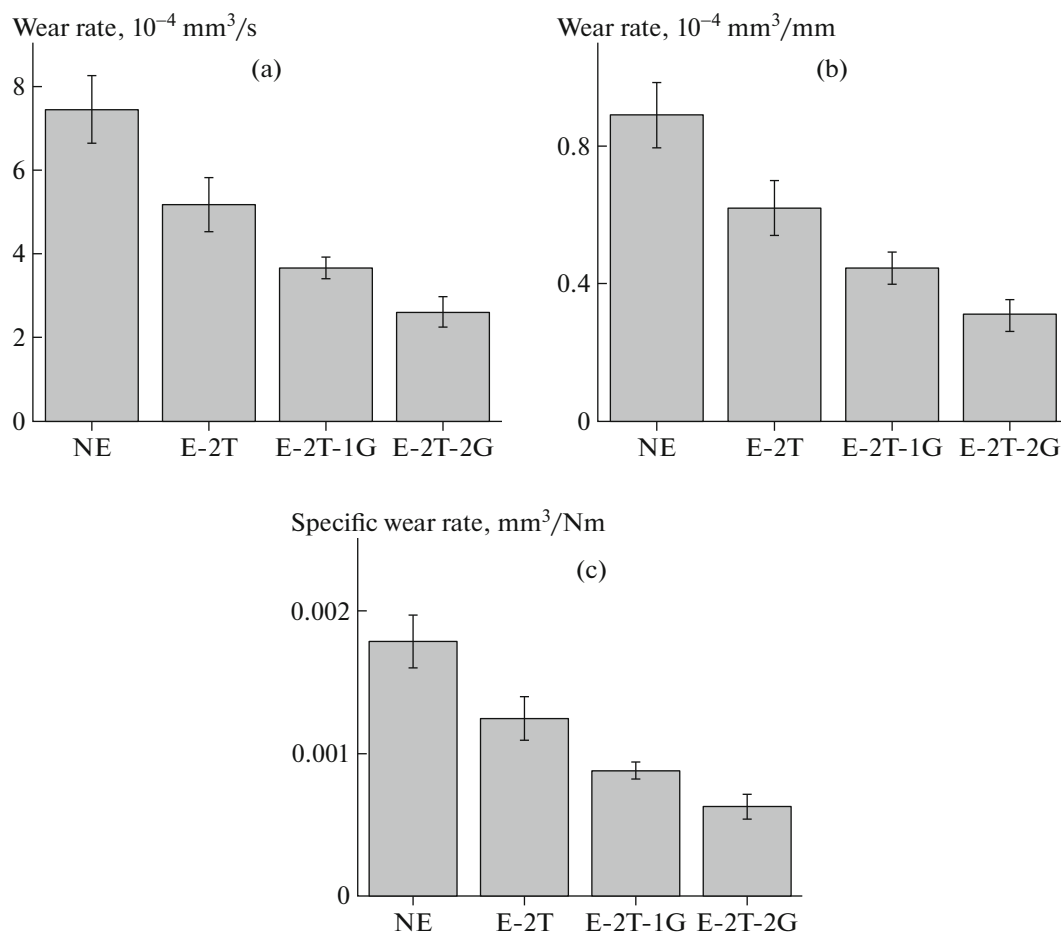


**Fig. 9.** Comparison of the (a) wear rate concerning time, (b) wear rate concerning distance, and (c) specific wear rate for various composite samples.

compressive peak stress values had increased by 15.28, 13.85 and 17.37%, respectively, as compared to neat epoxy. Thus, E-2T-2G samples showed the highest increase in compressive peak stress at this temperature. When tested at  $75^\circ\text{C}$ , NE, E-2T and E-2T-1G samples had approximately equal compressive peak stress, while the E-2T-2G sample showed a 7.54% decrease in compressive peak stress value. The difference between the thermal coefficient values of epoxy,  $\text{TiO}_2$  and GnP may be responsible for the decrease in the compressive peak stress of E-2T-2G sample. When the test was performed at  $120^\circ\text{C}$ , the peak stress of neat epoxy and nanocomposite samples decreased significantly compared to room temperature and  $75^\circ\text{C}$  in situ conditions. This may be attributed to increased polymeric chain mobility, as the temperature increased beyond the  $T_g$  of epoxy and nanocomposite samples (the  $T_g$  values of each configuration are further discussed in Thermal Analysis). The highest decrement was observed in the neat epoxy samples. Nanocomposites showed less decrement in peak stress values

mainly due to hindrance caused by nanofillers in polymeric chain movement.

The effect of increasing temperature on the compressive peak engineering stress of epoxy and nanocomposite samples has been shown in Fig. 12. It was found that each sample has its maximum compressive peak stress at ambient temperature, which goes on decreasing as we increase the temperature.

### Fractography

Some of the fractured samples were subjected to post-failure examination in order to better understand the various micro and nanoscale failure processes.  $\text{TiO}_2$  and GnP can considerably contribute to different strengthening and toughening mechanisms at the nanoscale, which can change the failure behavior of typical polymer composites. In addition, the in-service environment has a significant influence on the damage to micro-mechanisms in composite materials.

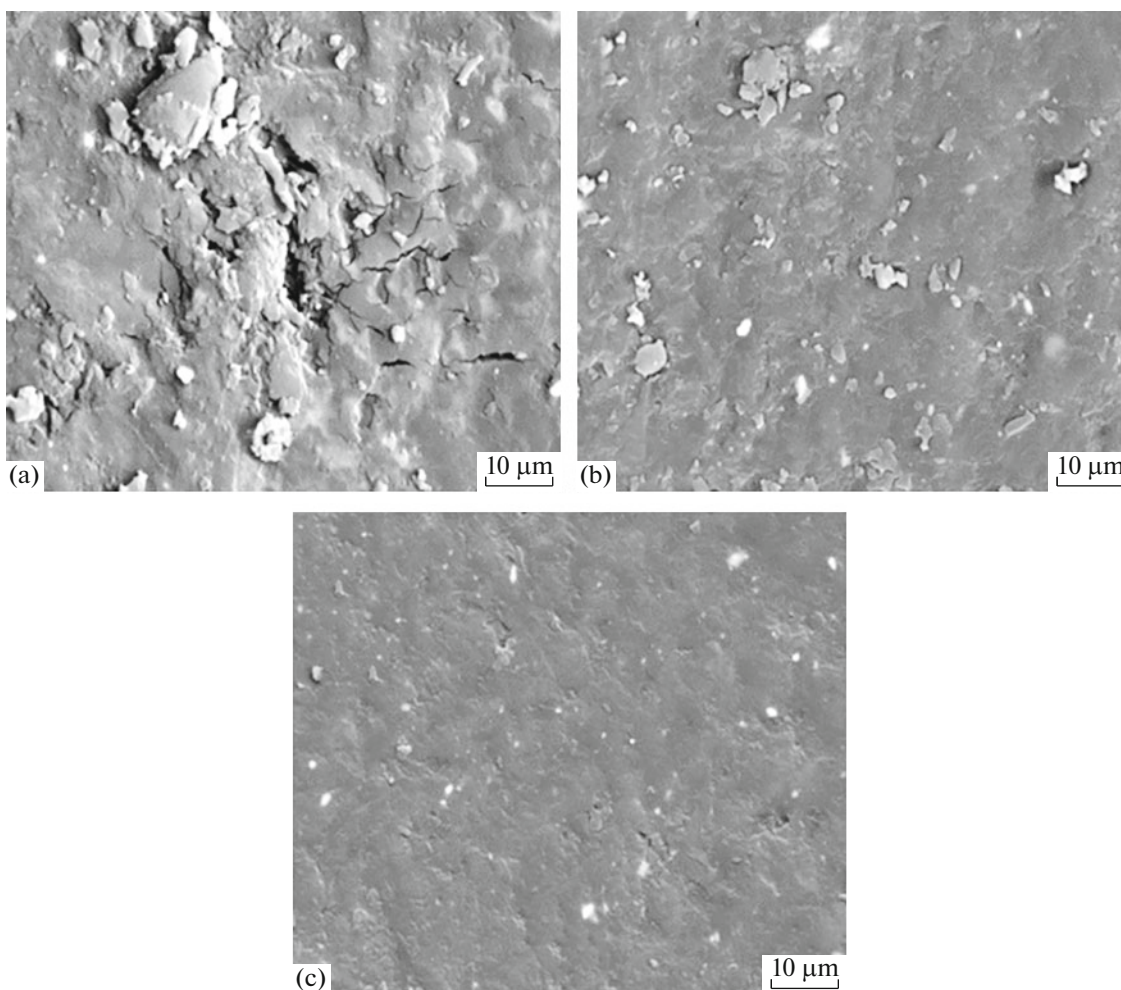
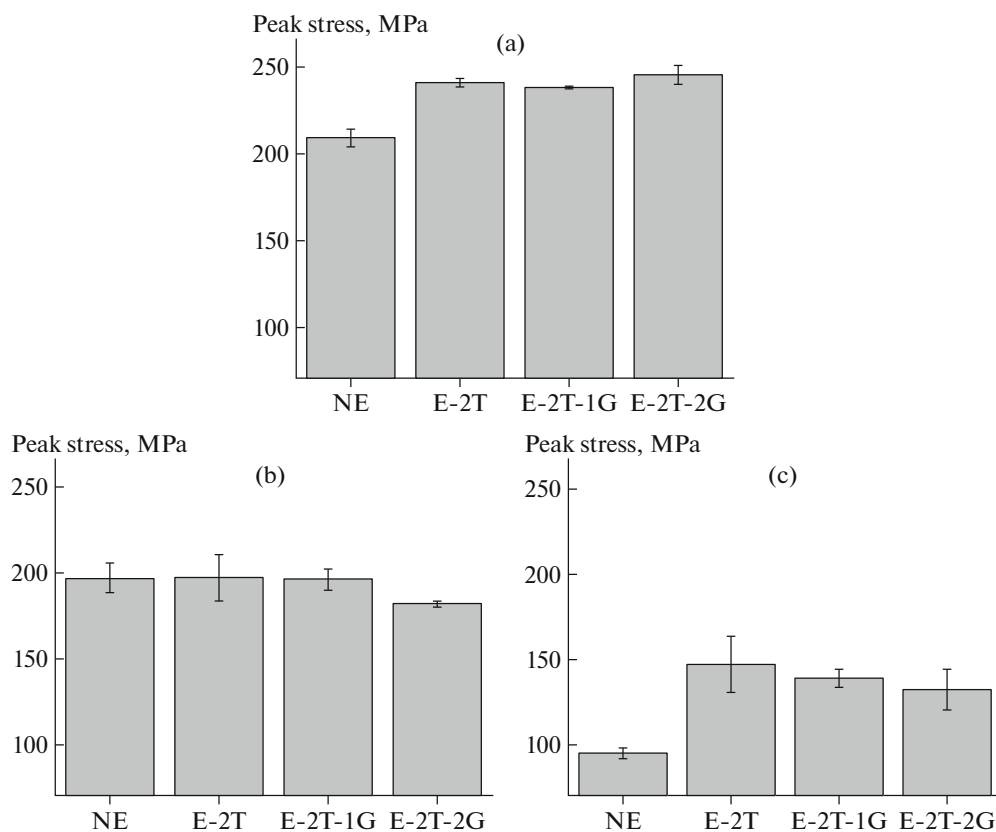


Fig. 10. SEM images of worn-out surfaces (a) NE, (b) E/2T, and (c) E/2T-2G.

The fractured (crushed) surfaces of the samples tested at 30 and 120°C are shown in Fig. 13. The fractured surface of NE at 30°C demonstrates a wide, smooth, homogeneous surface. The straight river line is not very intense. The SEM image indicates little resistance to fracture propagation. Compared to NE (tested at 30°C), E-2T-2G (tested at 30°C) reveals a rougher and less uniform surface, with more than one crack propagation route and more river lines. In this case, river lines are shorter and more packed, causing ribbons and fracture steps to diverge in different directions, dispersing stress and increasing crack resistance. The nanoparticle reinforced composites have rougher structured fracture surfaces, as seen in Fig. 13. Some toughening processes, such as localized inelastic shear matrix deformation and void nucleation, interfacial debonding, and crack deflection at agglomerates, are present in these nanocomposites because they are unaffected by filler particle shape [26]. At the testing temperature of 120°C for E-2T-2G, the crack growth was inhibited, which may be due to the inclusion of nanofillers, resulting in improved strength.

#### *Vickers Microhardness*

Vickers microhardness assessments were used to examine the impact of TiO<sub>2</sub> and GnP on the mechanical characteristics. It has long been considered a dependable characterization method for viscoelastic materials [30]. Vickers indentation has been found to be a useful method for probing hard polymeric materials such as epoxy-based composites due to the lack of recovery (elastic) along the diagonals [31, 32]. The value of Vickers hardness rose with the addition of nanofiller content in epoxy, as shown in Fig. 10. The maximum Vickers hardness value is attained by adding 2 phr TiO<sub>2</sub> and 2 phr GnP. Vickers hardness value for plain epoxy was found to be 20.07  $H_v$ . Figure 14 further demonstrates that E-2T composites have a microhardness value of 20.9, which is 4.14% higher than neat epoxy composites. When GNP (1phr and 2phr) is added, the corresponding hardness values are 23.3  $H_v$  and 24.32  $H_v$ , respectively, representing a 16.1 and 21.18% increase over pure epoxy. The increase in microhardness can be attributed to the interaction of



**Fig. 11.** Comparison of peak stress values of NE, E-2T, E-2T-1G, and E-2T-2G samples at (a) 30, (b) 75, and (c) 120°C.

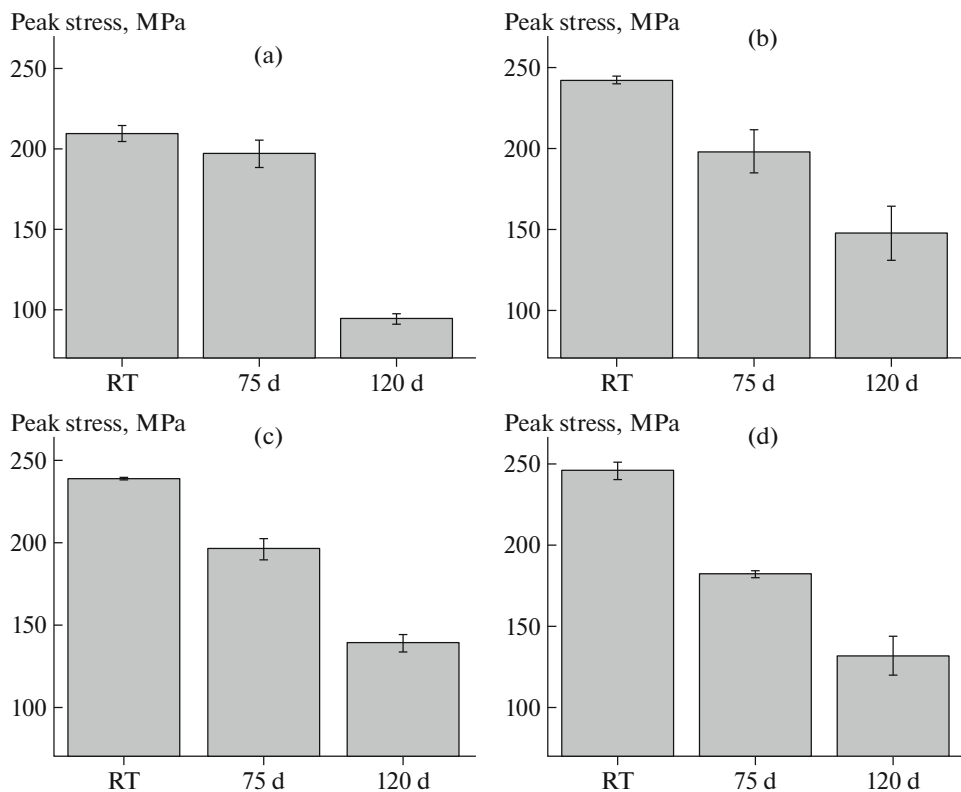


**Fig. 12.** Peak stress values of (a) NE at various temperatures, (b) E-2T at various temperatures, (c) E-2T-1G at various temperatures, and (d) E-2T-2G at various temperatures.

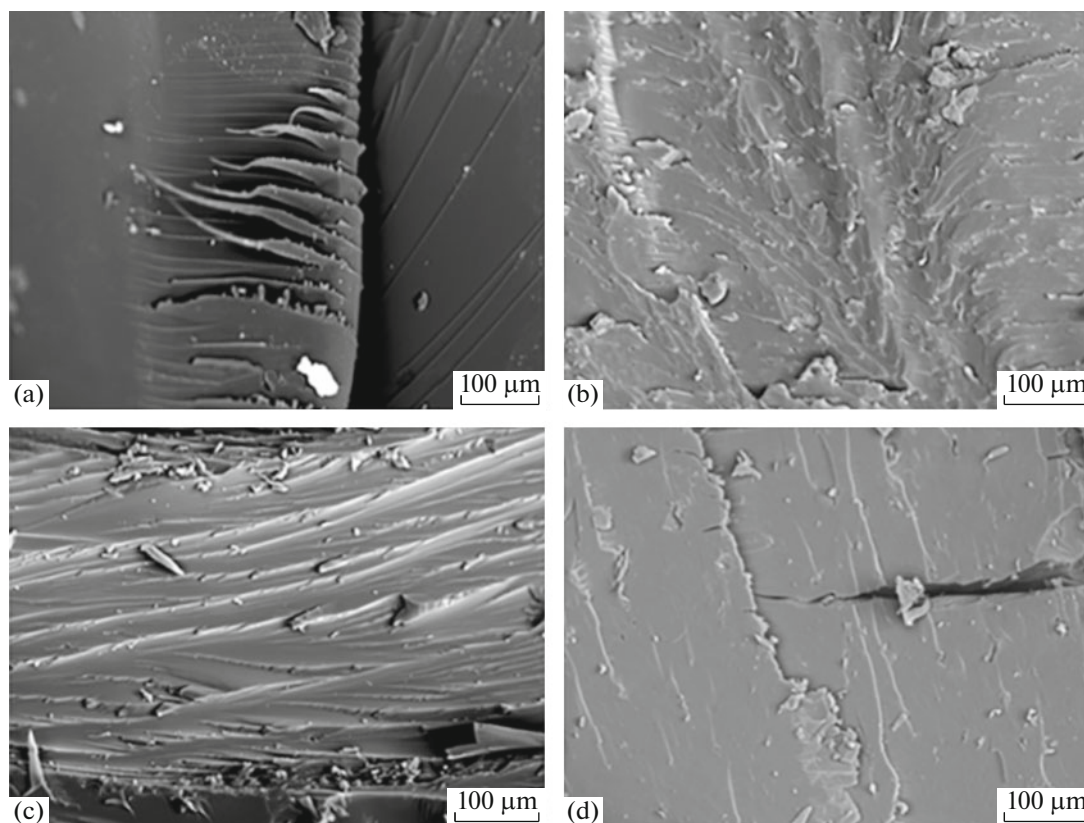


**Fig. 13.** SEM micrographs of the fractured surfaces of (a, c) NE and (b, d) E-2T-2G samples at (a, b) 30 and (c, d) 120°C.

fillers and matrix and effective stress transfer. At the same time, GnPs can raise the degree of crosslinking to limit segment mobility. The increment of the microhardness can also be accredited to the lack of aggregation sites inside composites that might have acted as stress concentration sites and substantially lower the mechanical characteristics.

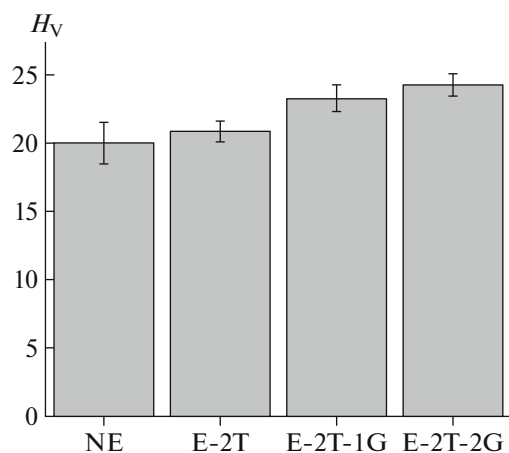


**Fig. 14.** Hardness measurement for different nanocomposite samples.

### Thermal Analysis

The glass transition temperature  $T_g$  of all the samples was systematically investigated, and the results are summarized in Fig. 15. Figure 15a shows the heat flow curve for each nanocomposite sample. The endotherm direction (downwards) shift of the heat flow curve represents the  $T_g$  of that material.  $T_g$  of neat epoxy was observed to increase with the addition of  $TiO_2$  and GnP. The absolute value of  $T_g$  may slightly vary with minute changes in the ambient environment during the hardening of polymer but broadly remains near the same value. The highest  $T_g$  was observed in the E-2T-1G sample, which is 7.5% higher than that of neat epoxy composite, as shown in Fig. 15b.  $T_g$  may have improved due to a decrease in chain segment mobility, induced by either a greater contact between  $TiO_2$  particles and the epoxy resin matrix or inhibited chain mobility owing to a large number of particles [33, 34]. The increased cluster size of linked  $TiO_2$ +GnP particles may be held responsible for the stagnation in  $T_g$  of the samples with further GnP particles added. Consequently, epoxy resin with 2phr  $TiO_2$  with 0, 1 and 2 phr GnP can enhance the  $T_g$  slightly.

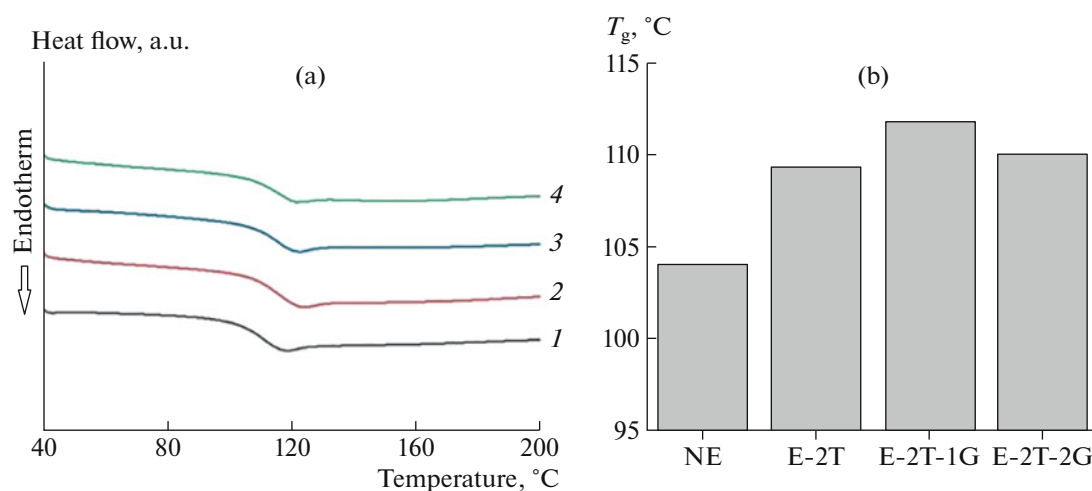


**Fig. 15.** DSC plot (a) heat flow vs temperature of (1) NE, (2) E-2T, (3) E-2T-1G, (4) E-2T-2G and (b) glass-transition temperature  $T_g$ .

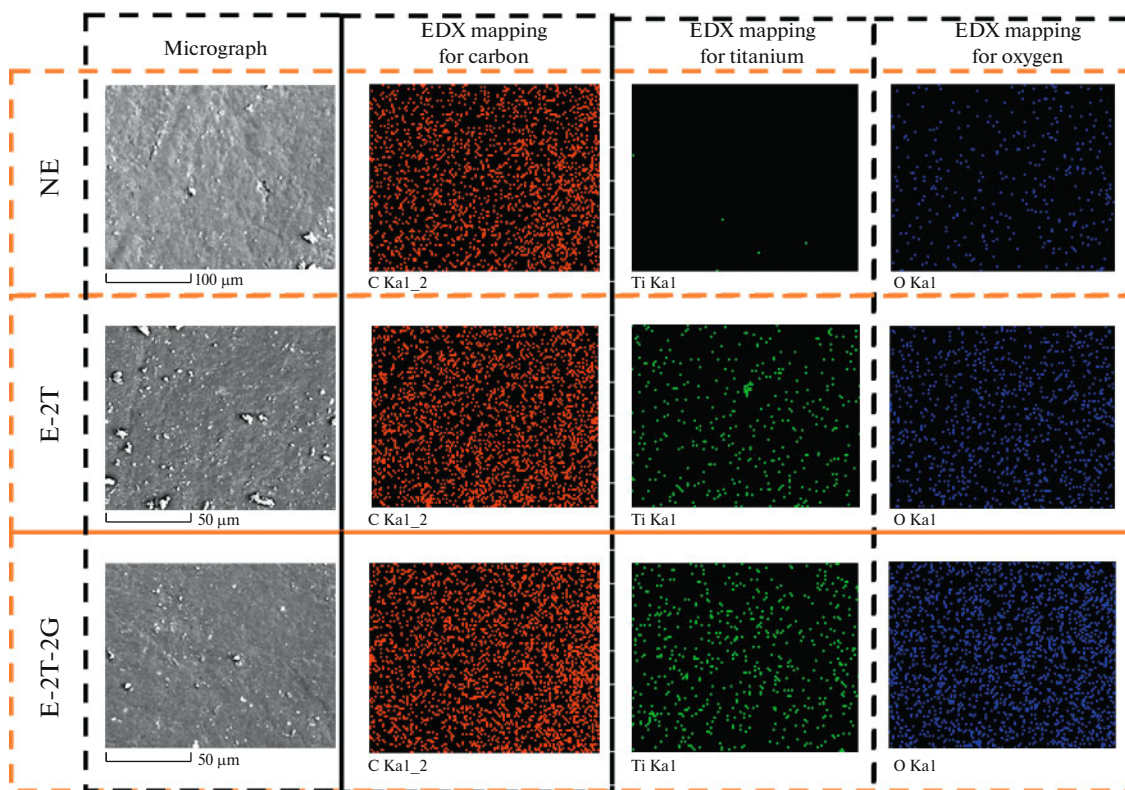


**Fig. 16.** EDX mapping for carbon, titanium and oxygen in different nanocomposite samples.

#### *EDX Analysis of Nanocomposite Surface*

EDX adjoined with the SEM was used to investigate the dispersion of nanoparticles. Figure 16 shows the SEM micrograph along with the elemental colored maps obtained using EDX for the nanocomposite samples NE, E-2T, and E-2T-2G. The main objective of the analysis was to check the dispersion and distribution

of nanoparticles within the matrix because the lower interfacial area and increased free volume in the composite due to poor particle dispersion can deteriorate the ultimate characteristics of nanocomposites [35]. For this, the dispersion of elements in the matrix was shown through red, green and blue dots for carbon, titanium and oxygen particles, respectively. The

figures suggest that there was no agglomeration of particles, indicating that a proper amount of nano-filler dispersion has been achieved. The satisfactory distribution of nanoparticles could be attributed to the low concentration of nanoparticles in the sample, which means that there is enough space between particles to prevent agglomeration. EDX mapping shows that as the weight fraction of nanoparticles increases, the amount of nanoparticle dispersion in the matrix intensifies. The interparticle distances decreased as the concentration of the nanoparticles increased, even then, agglomeration was not noticed.

### CONCLUSIONS

The wear and thermal behavior of binary nanofiller embedded epoxy-based nanocomposite samples were investigated. The wear analysis was conducted on a ball-on-disc setup, and it was observed that the addition of 2 phr GnP along with 2 phr TiO<sub>2</sub> showed maximum decreases in the wear volume by 65.1% when compared with neat epoxy. The SEM micrograph images obtained for the worn-out surface supported the result. The compressive peak stress values of the nanocomposite samples containing 2 phr TiO<sub>2</sub> along with 2 phr GnP were observed to be maximum at room temperature. The peak compressive stress decreases for all configurations when performing high-temperature compression loading. The surface microhardness was observed to be maximum for epoxy samples with 2 phr TiO<sub>2</sub> and 2 phr GnP, which was about 21.18% greater than the neat epoxy. The sample containing 2 phr TiO<sub>2</sub> along with 1 phr GnP showed the maximum  $T_g$ , which was about 7.5% higher than the Neat epoxy, whereas the  $T_g$  of the epoxy samples with 2 phr TiO<sub>2</sub> and 2 phr GnP was 5.77% higher than neat epoxy. Elemental colored mapping using EDX showed proper dispersion of nanofillers. Therefore, it is safe to say that using GnP and TiO<sub>2</sub> nanofillers in epoxy can enhance its wear resistance, surface hardness, and glass transition temperature.

### FUNDING

The authors would like to direct their deep sense of gratitude to the National Institute of Technology Rourkela and the Science and Engineering Research Board (SERB) of India (ECR/2018/001241) for providing infrastructural and financial support in completing this study.

### ACKNOWLEDGMENTS

The authors are also grateful for the technical assistance received from Mr. Rajesh Patnaik.

### CONFLICT OF INTEREST

The authors declare that they have no conflict of interest.

### REFERENCES

1. N. S. Hmeidat, J. W. Kemp, and B. G. Compton, *Compos. Sci. Technol.* **160**, 9 (2018).
2. B. Wetzel, F. Hauptert, and M. Qiu Zhang, *Compos. Sci. Technol.* **63**, 2055 (2003).
3. D. Pinto, L. Bernardo, A. Amaro, and S. Lopes, *Constr. Build. Mater.* **95**, 506 (2015).
4. S. S. Pendhari, T. Kant, and Y. M. Desai, *Compos. Struct.* **84**, 114 (2008).
5. M. K. Shukla and K. Sharma, *Polym. Sci., Ser. A* **61**, 439 (2019).
6. K. Kumar, P. K. Ghosh, and A. Kumar, *Composites, Part B* **97**, 353 (2016).
7. A. Jena, Shubham, R. K. Prusty, and B. C. Ray, *Mater. Today: Proceed.* **33**, 5184 (2020).
8. R. K. Nayak, A. Dash, and B. C. Ray, *Procedia Mater. Sci.* **6**, 1359 (2014).
9. R. K. Nayak, K. K. Mahato, and B. C. Ray, *Composites, Part A* **90**, 736 (2016).
10. S. Mohanty, Shubham, R. K. Prusty, and B. C. Ray, in *Processing and Characterization of Materials: Select Proceedings of CPCM 2020*, Ed. by S. Pal, D. Roy, and S. K. Sinha (Springer, Singapore, 2021), pp. 203–210.
11. S. Chatterjee, J. W. Wang, W. S. Kuo, N. H. Tai, C. Salzmann, W. L. Li, R. Hollertz, F. A. Nüesch, and B. T. T. Chu, *Chem. Phys. Lett.* **531**, 6 (2012).
12. A. Yu, P. Ramesh, M. E. Itkis, E. Bekyarova, and R. C. Haddon, *J. Phys. Chem. C* **111**, 7565 (2007).
13. Shubham, R. K. Prusty, and B. C. Ray, *Polym. Sci., Ser. B* (2022).  
<https://doi.org/10.1134/S1560090422700166>
14. F. Cilento, A. Martone, M. G. Pastore Carbone, C. Galiotis, and M. Giordano, *Compos. Sci. Technol.* **211**, 108873 (2021).
15. R. Wang, M. Aakyiir, A. Qiu, J.-A. Oh, P. Adu, Q. Meng, and J. Ma, *Polymer* **205**, 122851 (2020).
16. X. Sun, C. Huang, L. Wang, L. Liang, Y. Cheng, W. Fei, and Y. Li, *Adv. Mater.* **33**, 2001105 (2021).
17. D. K. Rathore, R. K. Prusty, D. S. Kumar, and B. C. Ray, *Composites, Part A* **84**, 364 (2016).
18. A. J. Crosby and J. Lee, *Polym. Rev.* **47**, 217 (2007).
19. J. Sumfleth, L. A. S. de Almeida Prado, M. Sriyai, and K. Schulte, *Polymer* **49**, 5105 (2008).
20. M. Nuruddin, R. Gupta, A. Tcherbi-Narteh, M. Hosur, and S. Jeelani, *Adv. Mater. Res.* **1119**, 155 (2015).
21. D. M. Kennedy and M. S. J. Hashmi, *J. Mater. Process. Technol.* **77**, 246 (1998).
22. E. M. Masoud, M. E. Hassan, S. E. Wahdaan, S. R. Elsayed, and S. A. Elsayed, *Polym. Test.* **56**, 277 (2016).
23. S. Khostavan, M. Fazli, M. G. Ahangari, and Y. Rostamiyan, *Adv. Polym. Technol.* **2019**, e8156718 (2019).
24. S. G. Prolongo, A. Jimenez-Suarez, R. Moriche, and A. Ureña, *Compos. Sci. Technol.* **86**, 185 (2013).

25. V. Kavimani, K. Soorya Prakash, T. Thankachan, and R. Udayakumar, *Composites, Part B* **191**, 107911 (2020).
26. P. Carballeira and F. Hauptert, *Polym. Compos.* **31**, 1241 (2010).
27. N. Hayeemasae, H. Ismail, S. Matchawet, and A. Masa, *Polym. Compos.* **40**, 3149 (2019).
28. J. D. Ambrósio, C. V. M. Balarim, and G. B. de Carvalho, *Polym. Compos.* **37**, 1415 (2016).
29. B. Satheesan and A. S. Mohammed, *Wear* **466–467**, 203560 (2021).
30. I. M. Low, *J. Eur. Ceram. Soc.* **18**, 709 (1998).
31. Y. Wang, J. Yu, W. Dai, Y. Song, D. Wang, L. Zeng, and N. Jiang, *Polym. Compos.* **36**, 556 (2015).
32. P. Bartolomeo, M. Irigoyen, E. Aragon, M. A. Frizzi, and F. X. Perrin, *Polym. Degrad. Stab.* **72**, 63 (2001).
33. K. H. Chen and S. M. Yang, *J. Appl. Polym. Sci.* **86**, 414 (2002).
34. K. Krzywiński, A. Sieradzki, Ł. Sadowski, A. Królicka, and C. Chastre, *Compos. Struct.* **282**, 115127 (2022).
35. M. Bayani, M. Ehsani, H. A. Khonakdar, J. Seyfi, and M. H. HosseinAbadi-Ghaeni, *J. Vinyl Addit. Technol.* **23**, E216 (2017).